Growth of room temperature ferromagnetic Ge1-xMnx quantum dots on hydrogen passivated Si (100) surfaces

Growth of room temperature ferromagnetic $Ge_{1-x}Mn_x$ quantum dots on hydrogen passivated Si (100) surfaces

Daniele Gastaldo, Gianluca Conta, Marco Coïsson, Giampiero Amato, Paola Tiberto, and Paolo Allia

Citation: AIP Advances **8**, 056414 (2018);
View online: https://doi.org/10.1063/1.5006881
View Table of Contents: http://aip.scitation.org/toc/adv/8/5
Published by the American Institute of Physics

Growth of room temperature ferromagnetic $Ge_{1-x}Mn_x$ quantum dots on hydrogen passivated Si (100) surfaces

Daniele Gastaldo,[1,2,a] Gianluca Conta,[1,3] Marco Coïsson,[1] Giampiero Amato,[1] Paola Tiberto,[1] and Paolo Allia[2]
[1]*Nanoscience and Materials division, Istituto Nazionale di Ricerca Metrologica, Torino 10135, Italy*
[2]*Applied science and technology department, Polytechnic University of Turin, Torino 10129, Italy*
[3]*Chemistry department, University of Turin, Torino 10125, Italy*

(Presented 9 November 2017; received 28 September 2017; accepted 10 November 2017; published online 27 December 2017)

A method for the synthesis of room-temperature ferromagnetic dilute semiconductor $Ge_{1-x}Mn_x$ ($5\ \% < x < 8\ \%$) quantum dots by molecular beam epitaxy by selective growth on hydrogen terminated silicon (100) surface is presented. The functionalized substrates, as well as the nanostructures, were characterized in situ by reflection high-energy electron diffraction. The quantum dots density and equivalent radius were extracted from field emission scanning electron microscope pictures, obtained ex-situ. Magnetic characterizations were performed by superconducting quantum interference device vibrating sample magnetometry revealing that ferromagnetic order is maintained up to room temperature: two different ferromagnetic phases were identified by the analysis of the field cooled – zero field cooled measurements.
https://doi.org/10.1063/1.5006881

I. INTRODUCTION

Nanosystems such as quantum dots (QDs) and nanowires have been intensively investigated for fundamental studies at the nanoscale, turning out to be versatile building blocks for present-day functional devices.[1] The possibility of combining tunability of semiconductor with properties of magnetic materials has been recognized for a long time as a promising route to explore new functionalities.

Heteroepitaxy of Ge/Si nanostructures is one of the most promising routes for realization of future nanoelectronics and nanophotonic devices. The discovery of room-temperature ferromagnetism in germanium manganese ($Ge_{1-x}Mn_x$) quantum dots obtained via heteroepitaxy on silicon[2] had attracted much attention due to the possibility to realize electric field control of ferromagnetism,[3] and indicates $Ge_{1-x}Mn_x$ alloys as good candidates for applications in spintronics.

Among semiconductor materials showing ferromagnetic features, $Ge_{1-x}Mn_x$ diluted alloys had attracted attention since the discovery reported in 2002 by Park et al.[4] of ferromagnetic order in a thin epitaxial layer of Mn-doped Ge, due to the huge variety of magnetic behavior that is linked to the tendencies of transition metal ions to segregate in the semiconductor host, forming ferromagnetic nanoclusters or nanocolumns.[5] These crystallites could be easily detected by magnetic characterization because they display a well-defined Curie temperature, usually much higher than that of the diluted phase: $T_C \sim 270$ K for Ge_3Mn_5 and $T_C \sim 296$ K for Ge_8Mn_{11}.[2,6]

In this work GeMn Quantum Dots have been successfully produced by heteroepitaxy on hydrogen passivated silicon surfaces displaying room temperature ferromagnetic behavior.

[a]Author to whom correspondence should be addressed. Electronic mail: daniele.gastaldo@polito.it

II. EXPERIMENT

Self-assembled Ge, SiGe and GeMn QDs are usually obtained exploiting the so called Stranski-Krastanov (SK) growth regime:[7,8] typically a thin germanium layer (2-3 nm) is deposited on the top of a silicon single crystal substrate held at high temperature (T > 750 K). This peculiar growth mode of the epitaxial layer is caused by the interplay between the lattice mismatch that exists between the substrate (lattice constant a_{Si} = 5.43086 Å[9]) and the epitaxial layer (a_{Ge} = 5.6574 Å[9]) and the strength of the chemical bond at the interface. At first, a continuous and homogeneously strained epitaxial layer of Ge is formed on the Si wafer, known as the wetting layer. The growth will continue with formation of 3D crystals (QDs), relaxing initial strain via formation of dislocations or by relaxation at the free surfaces of dots.[10]

To obtain a wetting layer followed by the SK growth, one must produce an atomically clean Si surface. This is typically achieved in UHV environment by thermal desorption (T > 800 °C) of a chemically grown SiO_2 layer from a clean Si substrate.[11] However, this process is not compatible with standard complementary metal-oxide-semiconductor (CMOS) fabrication processes. To overcome this issue a more recent technique[12] has been presented, which still contemplates deposition of $Ge_{1-x}Mn_x$ alloys onto a silicon substrate, having a hydrogen terminated surface.[13,14]

Etching Si (111) or Si (100) surfaces in diluted hydrofluoric acid (HF) solutions removes any oxide layer and produces stable and hydrogen terminated surfaces, since all surface Si atoms are fully coordinated. Surface morphology is strongly dependent on the etching solution pH and for pure HF diluted solutions (pH = 1-2) it was found that the resulting Si (100) surfaces are rough, (111)-faceted, and all the possible hydrides are presents (SiH, SiH_2 and SiH_3).[12]

After etching of substrates in HF diluted solution, it is possible to selectively remove the hydrogen from the dihydride and trihydride sites by thermal treatment. The resulting Si surface will provide some hydrogen free sites, corresponding to (100) planes, where the $Ge_{1-x}Mn_x$ dots start to nucleate selectively.

The hydrogen terminated silicon wafers for selective growth of $Ge_{1-x}Mn_x$ QDs have been prepared by etching the surface of 3-inches p-type, boron doped, Si (100) wafer (5 < ρ < 15 mΩ·cm) in diluted HF at the end of the following cleaning procedure:

1. Degrease in hot acetone for 10 min at 70 °C
2. Degrease in hot ethanol for 10 min at 70 °C
3. Rinse in deionized water
4. Boil in H_2O_2: H_2SO_4 (3:1) for 40 min at 70 °C
5. Rinse in deionized water
6. Etch in diluted (5%) HF solution for 10 s - 15 s at room temperature
7. Rinse in deionized water
8. Dry with nitrogen gas

Steps from 4 to 7 were repeated two times before loading the sample in a VG - Semicon molecular beam epitaxy apparatus ($P_{base} < 10^{-10}$ mbar). The sources were an e-beam for Ge and a Knudsen effusive cell for Mn. The Mn concentration was calibrated through XPS compositional measurements of thicker amorphous thin films,[15] while evaporation flux is monitored by using a movable Bayard-Alpert equivalent beam pressure ion gauge. Instead, the Ge deposition rate was measured and kept constant using a calibrated quartz crystal microbalance.

The sample was brought slowly to deposition temperature (T_{sub} = 590 °C), keeping pressure inside the deposition chamber in the 10^{-10} mbar range. Once the temperature is stabilized, Ge deposition started, with a rate of R_{Ge} = 4 Å/min together with Mn. The Mn flux was tuned to obtain a desired atomic concentration x ~ 8%, even if small variation in concentration (5 % < x < 8 %) are reported between different samples, having no impact on structural and magnetic properties. Final thickness measured by the quartz microbalance was h_{Ge} = 1.8 nm. Immediately after the growth, the sample was brought again to room temperature with a cooling rate of ~ 25 °C/min.

The as-grown sample of $Ge_{1-x}Mn_x$ was covered with a thin layer of polymethylmethacrylate (PMMA) (h=100 nm) immediately after the extraction from the MBE chamber to avoid any further oxidation before the magnetic characterization, while a portion of the same sample was left uncovered

for SEM inspection of wafer surface. Morphology of the samples was checked ex-situ via field emission scanning electron microscopy (FESEM) FEI Inspect F50. QDs mean diameter and the mean center to center distance have been evaluated.

Magnetic measurements have been performed in a Quantum Design's MPMS 3 SQUID-VSM. As the signals of an ensemble of nanometer sized DMS nanoparticles is of the order of 200 nemu, two 3×3 mm^2 square pieces were cut, stacked and fixed on the SQUID quartz sample holder to improve signal to noise ratio. Magnetic moment of the quartz rod was measured separately in the entire range of applied magnetic field values and then subtracted to the hysteresis loops.

To further reduce spurious contributions to the magnetic measurements of $Ge_{1-x}Mn_x$ we have removed the QDs from the substrate, by etching in H_2O_2 and then in a diluted HF solution (5%); subsequently, the SQUID measurements were carried out again, and the diamagnetic component coming from the same Si (100) substrates is directly measured.

Hysteresis loops were taken at 2.5 K, 10 K and 300K in the field range -7 T < H < 7 T. Field cooled - zero field cooled (FC-ZFC) curves were collected immediately after the measurement of isothermal hysteresis loops in the temperature interval 2.5 K < T < 300 K by using the standard procedure with an applied field H = 50 Oe.

III. RESULTS AND DISCUSSION

Before and during growth, reflection high energy electron diffraction (RHEED) pattern was continuously checked. The results are shown in Figure 1(a), (b) and (c). Room-temperature RHEED diffraction patterns from the substrate, taken with an accelerating voltage of 13 kV are shown in Figure 1 (a, b): the 1×1 surface reconstruction pattern is visible as expected for hydrogen passivated silicon surfaces.[12] To maintain a low degree of substrate roughness the immersion time in diluted HF solution (Step 6) was minimized to 10-15 seconds. Indeed, this time is enough to obtain a strong hydrophobic silicon surface without introducing too much roughness; as a result, Kikuchi lines are intense and well developed in patterns coming from these surfaces, meaning that roughness is maintained on an atomic level.

The RHEED pattern at the end of growth process is displayed in figure 1(c): at this stage (h_{Ge}= 1.8 nm) the pattern is very intense, Kikuchi lines are completely lost because surface roughness is increased. For a Ge crystal growing on a Si (100) surface epitaxially we expect to see in

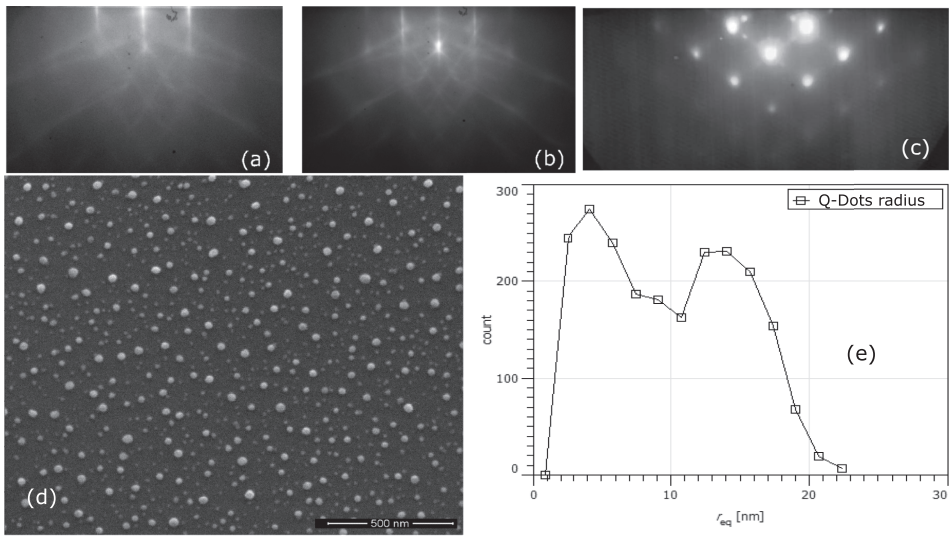

FIG. 1. RHEED patterns (13 keV electron beam) from a clean hydrogenated silicon (100) surface taken along the <001> (a) and the <011> azimuthal directions (b) and from a $Ge_{1-x}Mn_x$ Q-Dots growth along the <011> azimuth; (d) SEM pictures of $Ge_{1-x}Mn_x$ QDs taken with an accelerating voltage of 10 kV and (e) equivalent radii distribution obtained through the Otsu thresholding procedure extended over the surface represented in figure (d).

transmission a square lattice projected on the screen (rotated by 45°), this because periodicity between horizontal and vertical planes of a Ge (100) surface should be the same. On the contrary, we observe a centered rectangular lattice (figure 1(c)); this originate from strain-induced deformation of the zinc-blend lattice, which is elongated in the vertical direction and hence, in reciprocal space, is squeezed along the horizontal one. In this pattern twinned spots are observed also; these are caused by the presence of defects in the growth of the nanocrystals due to wrong stacking of crystalline plane. A twin implies that bonds between atoms are the correct ones but the crystal is growing in more than one direction with the same orientation. These symmetrical intergrowths of crystals are called twinned crystals.[16]

A representative SEM image of $Ge_{1-x}Mn_x$ QDs sample surface is shown in figure 1(d); a good and homogeneous coverage of small nanocrystals is observed. Nevertheless, the distribution of the dots size appears to be quite broad. The picture in figure 1(d) was further analyzed using clustering-based image thresholding, exploiting Otsu's method. This analysis, presented in figure 1(e), was carried out on a surface of 12×10^{-8} cm^2 and confirmed that distribution of dots equivalent radii is broad indeed (2 nm < r < 22 nm). However, two peaks could be identified: one centered at r ~ 4 nm and a second at r ~ 15 nm. The dot density and the mean center to center distance between the nanocrystals were also extracted from the same area; these values are respectively: $\rho = 1.87\times10^{10}$ cm^{-2} and, $d = 1/\rho^{1/2} = 73$ nm. Almost equivalent values were reported for the growth of SiGe QDs in similar growth conditions (80 nm < d < 90 nm, $\rho = 1\times10^{10}$ nm) for dot with a typical half base of 20 nm, pointing out that Mn does not impact in a severe way the nanocrystals growth process.

Magnetic analysis of the same sample $Ge_{1-x}Mn_x$ with h_{Ge} = 1.8 nm is presented in figure 2(a), (b) and (c). Since the sample is composed of nanometer size crystalline particles dispersed on a substrate we expect that, if the particles are ferromagnetic, a superparamagnetic regime should appear. In order to assess the magnetic properties of these nanomagnets, zero field cooling-field cooling curves (ZFC-FC) were measured in addition to isothermal hysteresis loops. To reduce the possible

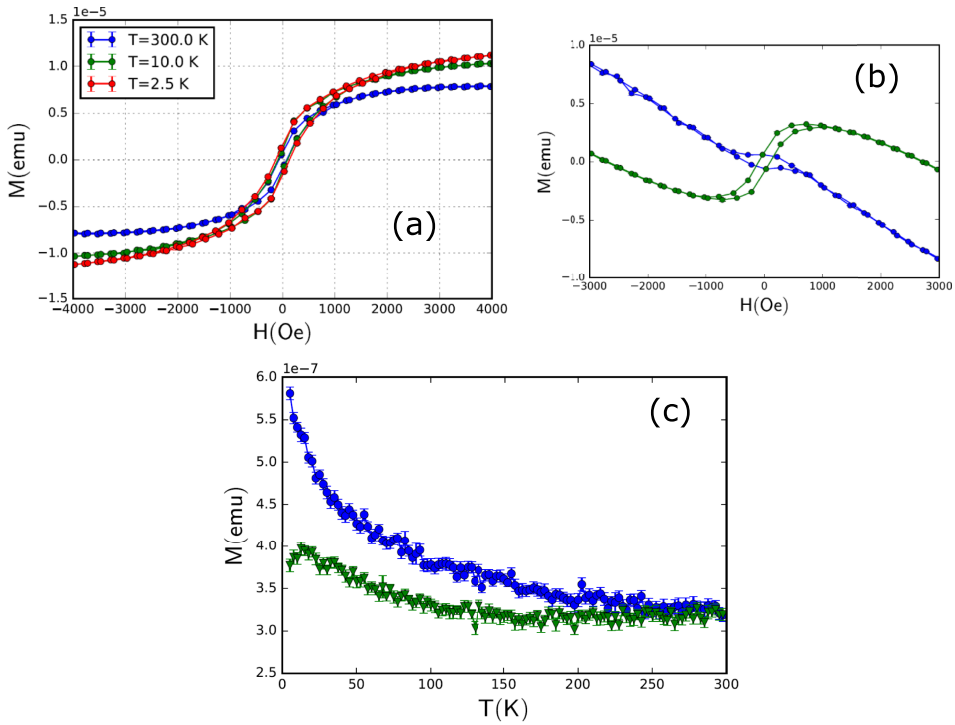

FIG. 2. (a) hysteresis loops measured at different temperatures of the $Ge_{1-x}Mn_x$ (x ~ 8%) QDs after the subtraction of the signal coming from the substrate, (b) hysteresis loops at 300 K of the base substrate after the QDs removal (Blue) and the substrate plus the QDs (Green) and (c) FC (blue dots) and ZFC (green triangles) curves taken on sample $Ge_{1-x}Mn_x$ (x ~ 8%) under a field of 50 Oe in temperature range 2.5 K < T < 300 K.

spurious contributions to the magnetic properties of QDs we repeated the measurements after removing them from the substrate. Some residual hysteresis was observed indeed, as shown in figure 2(b), with a coercivity almost as large as those of the complete sample. The source of this residual signal may be attributed to the presence of a small fraction of ferromagnetic contaminants in the substrate. However, after proper compensation of the magnetic signal from the substrate, hysteresis loops show a well-defined ferromagnetic behavior. The coercive field value extracted from three measured hysteresis loops, visible in figure 2(a), are H_C (300 K) ~ 80 Oe, H_C (10 K) ~ 110 Oe and H_C (2.5 K) ~ 140 Oe.

The value of the saturation moment at 300 K is $M_S = 7.8\times10^{-6}$ emu corresponding to about 8.5×10^{15} μ_B. Mn is expected to bring in a magnetic moment roughly equal to 3 μ_B per atom when diluted in Ge matrix, as well as in the case of the Ge_3Mn_5 ferromagnetic phase.[17] Total volume of deposited Ge can be estimated as $V_{Ge} \cong 5\times10^{-8}$ cm^3. Therefore, the concentration of Mn extracted from magnetic measurement at 300 K is of the order of 10%. However, this value is just an estimate because it is hard to precisely know the total volume of QDs as well as the total fraction of Mn atoms that participate in the ferromagnetic phase.

In the ideal case of monodisperse nanoparticles, having a narrow size distribution, the system performs the transition between irreversible and reversible regime in a correspondingly narrow temperature region marked by the sharp peak of the ZFC curve; just above this, the FC and ZFC curves merge. On the contrary, in our sample (figure 2c) the ZFC-FC curves exhibit two major features: the two curves start to diverge at T ~ 250 K, while a peak of the ZFC is visible at T ~ 13 K.

The sample having been grown at relatively high temperatures (Tsub = 590 °C), we cannot exclude the presence of a stoichiometric ferromagnetic compound with high T_C, such as Ge_3Mn_5, which can easily form in this condition. However, Ge_3Mn_5 usually forms particles much larger than the ones observed here;[18] on the other hand, the features of the ZFC/FC curves can be explained considering that the blocking temperature for superparamagnetic nanoparticles is proportional to $1/K_{eff}V$, where K_{eff} is the effective material magnetic anisotropy constant and V is the volume of the superparamagnetic nanoparticles. As a consequence, it is expected that the population of these superparamagnetic particles, which appears broadly distributed relying on SEM inspection, has a considerable distribution of blocking temperatures. Therefore, it is likely that a significant fraction of the particles with size near to the higher peak of the equivalent radii distribution (figure 1(e)) are already blocked at high temperature, giving rise to the irreversibility of the ZFC-FC that appears at T ~ 250 K. By further lowering the temperature, smaller nucleation sites eventually freeze out, originating the peak of the ZFC curve at about 15 K, that represents the mean blocking temperature of the smaller population of QDs. The value of the effective anisotropy constant of small nanoparticles, estimated from the blocking temperature T_B through the standard expression $K_{eff}=25k_BT_B/V$, turns out to be of the order of 1 x 10^5 erg/cm^3 for nanoparticles with radii of 5 nm. This value indicates that the small nanoparticles in our sample are not made of the Ge_3Mn_5 phase, which is known to display a much higher value of K_{eff}. In particular, K_{eff} values of 1.4 x 10^6 erg/cm^3 and 4.1 x 10^6 erg/cm^3 have been reported in Ge_3Mn_5 nanoparticles of similar size (11 nm compared to 5-14 nm) and in Ge_3Mn_5 nanocolumns (in this case, only the magneto-crystalline contribution is taken into account).[19,20] The magnetic moments at 300 K do not drop to zero, suggesting a high T_C of the DMS QDs, as also confirmed by the well-developed hysteresis of the magnetic loop observed at T=300 K.

IV. CONCLUSIONS

Germanium manganese QDs have been successfully grown on hydrogen-passivated Si (100) surfaces. By exploiting this technique, it is possible to eliminate the high-temperature step required for the SK growth on oxidized silicon substrates,[11,12] making this process much more attractive for compatibility with standard CMOS process. Size distribution is quite broad, but its upper limit (r ~ 22 nm) is sufficiently small to guarantee quantum confinement that can play a role in their physical properties.[1]

Analysis of the magnetic properties revealed that hysteresis could be observed in the magnetization loop even at room temperature. The ZFC-FC curves show a superparamagnetic blocking

temperature at low temperature ($T_B \sim 15$ K) and irreversibility starting at $T \sim 250$ K ascribed to the broad size distribution of the QDs.

[1] T. Dietl and H. Ohno, Rev. Mod. Phys. **86**, 187 (2014).
[2] F. Xiu, ISRN Condens. Matter Phys. **2012**, 1 (2012).
[3] F. Xiu, Y. Wang, J. Kim, A. Hong, J. Tang, A. P. Jacob, J. Zou, and K. L. Wang, Nat. Mater. **9**, 337 (2010).
[4] Y. D. Park, A. T. Hanbicki, S. C. Erwin, C. S. Hellberg, G. Spanos, and B. T. Jonker, Science (80) **295**, 651 (2002).
[5] M. Jamet, A. Barski, T. Devillers, V. Poydenot, R. Dujardin, P. Bayle-Guillemaud, J. Rothman, E. Bellet-Amalric, A. Marty, J. Cibert, R. Mattana, and S. Tatarenko, Nat. Mater. **5**, 653 (2006).
[6] R. B. Morgunov, A. I. Dmitriev, and O. L. Kazakova, Phys. Rev. B - Condens. Matter Mater. Phys. **80**, 1 (2009).
[7] I. V. Markov, *Crystal Growth for Beginners*, 2nd Edition. (2004).
[8] T. Nie, J. Tang, and K. L. Wang, J. Cryst. Growth **425**, 279 (2015).
[9] S. M. Sze, Physics of Semiconductor Devices (1969).
[10] D. J. Eaglesham and M. Cerullo, Phys. Rev. Lett. **64**, 1943 (1990).
[11] A. Ishizaka, J. Electrochem. Soc. **133**, 666 (1986).
[12] V. Le Thanh, T. T. T. Ngo, H. Bui, D. Bouchier, T. T. T. Le, and K. H. Phan, Thin Solid Films **428**, 144 (2003).
[13] E. Yablonovitch, D. L. Allara, C. C. Chang, T. Gmitter, and T. B. Bright, Phys. Rev. Lett. **57**, 249 (1986).
[14] M. Grundner and H. Jacob, Appl. Phys. A **39**, 73 (1986).
[15] G. Conta, G. Amato, M. Coïsson, and P. Tiberto, Sci. Technol. Adv. Mater. **18**, 34 (2017).
[16] G. Dhanaraj, K. Byrappa, V. Prasad, and M. Dudley, editors, *Handbook of Crystal Growth* (n.d.).
[17] C. Zeng, S. C. Erwin, L. C. Feldman, A. P. Li, R. Jin, Y. Song, J. R. Thompson, and H. H. Weitering, Appl. Phys. Lett. **83**, 5002 (2003).
[18] D. Bougeard, S. Ahlers, A. Trampert, N. Sircar, and G. Abstreiter, **237202**, 95(2006).
[19] S. Zhou, W. Zhang, A. Shalimov, Y. Wang, Z. Huang, D. Buerger, A. Mücklich, W. Zhang, H. Schmidt, and M. Helm, Nanoscale Res. Lett. **7**, 528 (2012).
[20] A. Jain, M. Jamet, A. Barski, T. Devillers, C. Porret, S. Gambarelli, V. Maurel, A. Jain, M. Jamet, A. Barski, T. Devillers, and C. Porret, **202502**, 1 (2010).